



INSTITUTE OF COGNITIVE SCIENCE  
BIOLOGICALLY ORIENTED COMPUTER VISION GROUP

*Master's Thesis*

**Nodule Detection in Lung CT Scans with  
Deep Learning**

Andrea Suckro

December 8, 2017

First supervisor: Dr. Ulf Krumnack  
Second supervisor: Prof. Dr. Gunther Heidemann

## **Nodule Detection in Lung CT Scans with Deep Learning**

This thesis makes use of a 3D Convolutional Deep Neural Network to classify whether a certain lung region contains a nodule or not. The network is trained on an open dataset containing roughly 1000 patient's full lung scan. The network is analyzed, its features visualized and compared to already existing solutions.

# Contents

|          |  |           |
|----------|--|-----------|
| <b>1</b> | <b>Introduction</b>                      | <b>5</b>  |
| 1.1      | Medical Context . . . . .                | 5         |
| 1.2      | Current Medical Approach . . . . .       | 5         |
| 1.3      | Opportunities for Assistance . . . . .   | 7         |
| 1.4      | The Problem of Neural Networks . . . . . | 8         |
| 1.5      | Structure of this thesis . . . . .       | 8         |
| <b>2</b> | <b>Dataset</b>                           | <b>9</b>  |
| 2.1      | Content and Structure . . . . .          | 9         |
| 2.1.1    | Scan Data Structure . . . . .            | 9         |
| 2.1.2    | Annotation Structure . . . . .           | 10        |
| 2.2      | Preprocessing . . . . .                  | 12        |
| 2.2.1    | Reading in the data . . . . .            | 12        |
| 2.2.2    | Slicing the patches . . . . .            | 13        |
| <b>3</b> | <b>Current Approaches</b>                | <b>14</b> |
| 3.1      | Classical Approaches . . . . .           | 14        |
| 3.1.1    | Segmentation . . . . .                   | 14        |
| 3.1.2    | Candidate Selection . . . . .            | 15        |
| 3.1.3    | Classification . . . . .                 | 16        |
| 3.2      | Deep Learning Approaches . . . . .       | 17        |
| 3.3      | This Thesis . . . . .                    | 17        |
| <b>4</b> | <b>Methods</b>                           | <b>18</b> |
| 4.1      | Software Packages . . . . .              | 18        |
| 4.2      | Convolutional Neural Network . . . . .   | 18        |
| 4.2.1    | Convolutional Layer . . . . .            | 19        |
| 4.2.2    | Dense Layers . . . . .                   | 20        |
| 4.3      | Training . . . . .                       | 20        |
| <b>5</b> | <b>Methods</b>                           | <b>23</b> |
| 5.1      | Software Packages . . . . .              | 23        |
| 5.2      | Convolutional Neural Network . . . . .   | 23        |
| 5.2.1    | Convolutional Layer . . . . .            | 24        |

|                   |   |           |
|-------------------|---|-----------|
| 5.2.2             | Dense Layers . . . . .                      | 25        |
| 5.3               | Training . . . . .                          | 25        |
| <b>6</b>          | <b>Results</b>                              | <b>28</b> |
| 6.1               | The trained Network . . . . .               | 28        |
| 6.2               | Analyzing the Network . . . . .             | 28        |
| 6.2.1             | Mean Class Activation . . . . .             | 28        |
| 6.3               | Bridge to other Approaches . . . . .        | 28        |
| <b>7</b>          | <b>Discussion</b>                           | <b>31</b> |
| 7.1               | Items of future code optimization . . . . . | 31        |
| 7.2               | Items of future investigation . . . . .     | 32        |
| <b>Appendices</b> |   | <b>I</b>  |
| <b>A</b>          | <b>Software</b>                             | <b>I</b>  |
| A.1               | Python . . . . .                            | I         |
| A.2               | Oracle Grid Engine . . . . .                | I         |
| A.3               | Tensorflow . . . . .                        | III       |
| <b>B</b>          | <b>Data</b>                                 | <b>V</b>  |
| B.1               | LIDC-IDRI Dataset . . . . .                 | V         |
| B.2               | CT Scanner Technology . . . . .             | V         |
| B.3               | CT Specifications . . . . .                 | VI        |

# Chapter 1

## Introduction

This master thesis centers around the automated detection of nodules in lung region CT scans. The introduction will cover the medical context necessary to understand the problem and motivate the use of Deep Neural Networks to assist in the task of nodule detection. It also explains the research question at hand and the structure of the thesis with an overview of the sections to come.

### 1.1 Medical Context

In 2012 34,490 men and 18,030 women in Germany were diagnosed with an illness corresponding to the ICD-10 code C33-34 [KSK<sup>+</sup>15]. This code describes malignant tumors in the breathable tract more generally summarized as lung cancer. 43,499 people died from this illness, which makes it one of the most dangerous types of cancer in Germany. The international comparison shows that other countries too suffer under its impact (see Figure 1.1).

The main risk factor has been shown to be the exposure to tobacco smoke, whether it's active consumption via cigarettes, or passive exposure especially in closed rooms. CT scanners are used to detect irregular tissue in a patient's lung region. These irregularities are grouped under the term *pulmonary nodule*. A pulmonary nodule is a small, round (parenchymal) or worm (juxtапleural) shaped lesion in the lungs. Each lesion has a chance to be malignant and may grow and spread over time, becoming a risk for the patient's life in the form of lung cancer. Nodules come not only in different shapes but differ along other features as well. Ground-glass opacity (GGO) nodules are a challenging kind of nodules since they are not thoroughly solid and so harder to detect on a CT scan. The location of the nodules is crucial for the detection rate since nodules close to bigger vessels or the chest wall do not differ much in intensity to the surrounding tissue and can be easily overlooked by the radiologist.

### 1.2 Current Medical Approach

In the clinical setting, the supervising medical staff has additional information available apart from the CT scans. Patients are either in a high-risk group (over a certain age and heavy

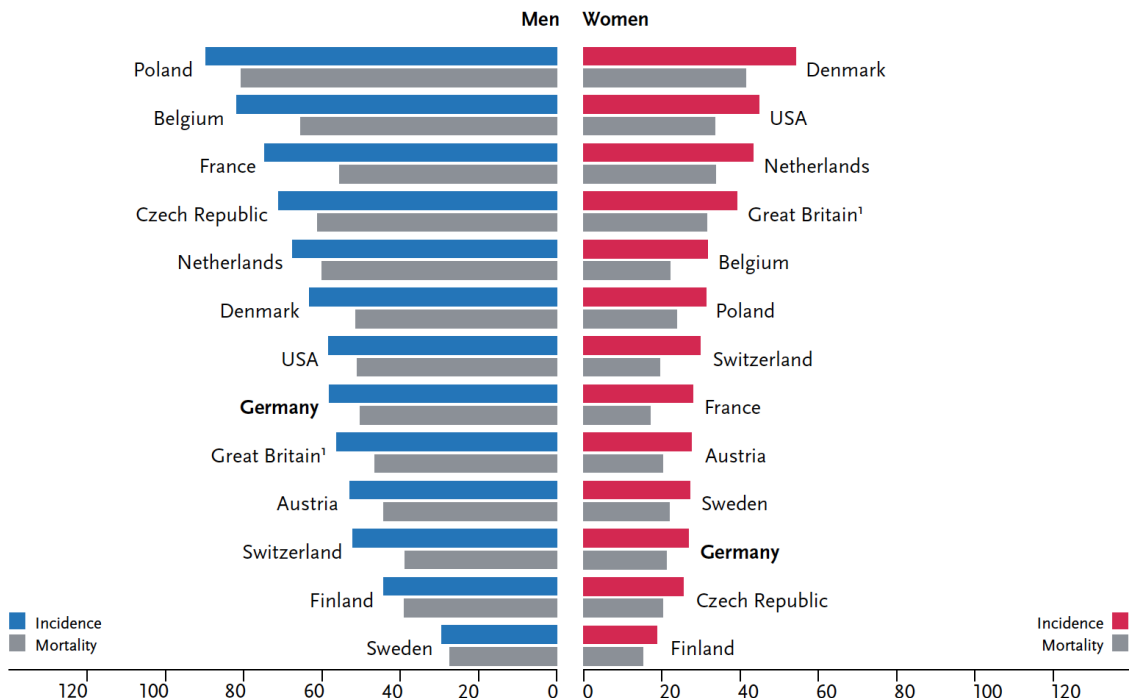


**Figure 1.1:** International comparison of age-standardized incidence and mortality rates for lung cancer in the year 2012

smokers) or present certain syndromes like fatigue, weight loss, cough, dyspnea, hemoptysis and chest pain. Different methods are used to find the underlying cause of these symptoms:

**Sputum cytology** Sputum is mucus that is produced in the lower airways which can be analyzed for bacteria and irregular cells.

**Biopsy** In a biopsy tissue samples are directly taken from the lung of the patient. This may be done in several ways, either bronchoscopic (obtaining the sample with an instrument through the airways) or directly by a needle or incision through the chest wall.

**Imaging tests** different imaging techniques are available for analyzing the lung: a regular X-Ray scan, but also MRI. The data used in this thesis stems from LDCT scans which stand for *low-dose computed tomography*. The radiation used in this method lies around 2.35 mSv which corresponds to roughly 80% less radiation than regular CT scans [OHO<sup>+13</sup>].

Lung cancer is tricky to detect since the symptoms show up very late in the process of the illness and it is often too late for the patient when those are recognized. Sputum cytology and biopsy are only used when there is already circumstantial evidence (like other symptoms) for lung cancer which may often be too late in the development of the illness for a successful treatment. This makes imaging techniques the only source for early detection. Radiologists are required to analyze roughly 100-600 pictures per patient depending on the slice thickness

of the used technique and the body height of the patient. Medical image viewers like OsiriX (Figure 1.2) are assisting in this process and have also been used in this thesis to analyze the image data.

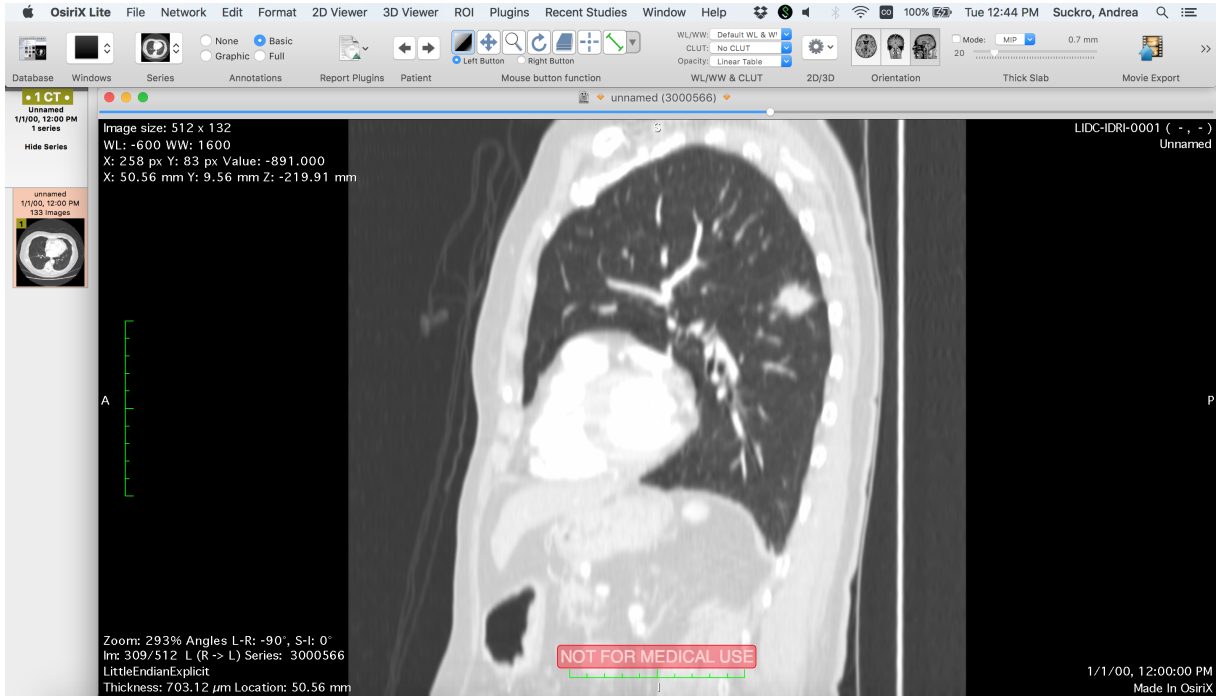


**Figure 1.2:** Screenshot of the analyzing software OsiriX. It is the most widely used software in the domain of medical image viewers and offers a free trial version that was used for this thesis.

Yet it is still a highly complicated task and despite all efforts in this field the process is of course not fail-safe and it can happen that nodules are not detected in an early stage of their development but later when a successful treatment is not as likely anymore. A study by Kakinuma et. al. [KAK<sup>+12</sup>] shows how different features like the slice thickness and the nodule properties affect the detection rate, dropping it to 65.5% for pure ground-glass opacities in a scan with 2mm slice thickness. Another issue arises with the false positive rate. A study by Pinsky et. al. [PGN<sup>+13</sup>] reports a mean false positive rate of 28.7% across 112 radiologists at 32 screening centers in and outside of the US. This puts additional stress on the patient and requires further tests to conclude that there is no cancer present.

### 1.3 Opportunities for Assistance

Early detection of lung cancer is important in two ways. First, it increases the chance of a successful treatment and secondly, it avoids unnecessary scans in the scenario of undetected cancerous material or wrongly classified abnormalities in the lung. As the number of preventive screening procedures rises and the used scanners become more granular software-based assistance becomes a helpful companion to every radiologist [LAS<sup>+05</sup>].

The scientific literature provides many algorithmic approaches to finding nodules in CT Scans [AGM<sup>+</sup>99] [AGM01] [OCK05] [TLD<sup>+</sup>09] [YLD<sup>+</sup>09] using handcrafted features and in-depth knowledge of the structure of the data and the nodules that should be detected. Some make already use of Deep Convolutional Neural Networks to solve this or related tasks (like classifying the malignancy of a nodule) [CNC<sup>+</sup>16] [HSV17] [SZY<sup>+</sup>15].

Despite many efforts being devoted to the computer-aided nodule detection problem, lung CAD systems remain an ongoing research topic. One of the major difficulties is the detection of GGO nodules with low-dose thin-slice CT screening. Another two difficulties are the detection of nodules that are adjacent to vessels or the chest wall when they have very similar density and the detection of nodules that are nonspherical in shape. In such cases, classical approaches like intensity thresholding or model-based methods might fail to identify the nodules correctly.

## 1.4 The Problem of Neural Networks

Neural Networks are strong tools that *solve* many tasks with astonishing performance (see for example [SSS<sup>+</sup>17]). Yet it seems like the solution they come up with is not intelligible to humans in the same way as (for example) a feature detector that was directly designed to respond to geometric properties of the nodule. But in a scenario where medical decisions are based on the output of an algorithm, it is crucial that the algorithm is reliable and the way it comes up with a decision is accepted by the people responsible. As long as this is not the case the people working with the software will not completely accept its value and it can not be ruled out that the network produces erroneous results in cases that did not occur during the training phase.

In this thesis, a Deep Neural Network will be developed that uses 3D CT scan information to classify a given CT image patch as either containing a nodule or not. Then mechanisms will be applied to visualize the learned features and discussed whether they can be conceptualized in terms of already approved procedures. The problem in this sense is two-fold. First - can a 3D Convolutional Neural Network solve the task of nodule detection and second, how can it's solution to the problem be understood?

## 1.5 Structure of this thesis

This thesis is structured in the following way: in chapter 2 the used dataset is described as well as it's preprocessing for the learning algorithm. The 3rd chapter will give an overview over the field and explain some of the current computational approaches that are used for detecting nodules. The methods chapter 5 contains information about the used software packages that were necessary to implement the algorithms as well as information about Convolutional Neural Networks and the model that is presented and analyzed in chapter 6. That chapter focuses on extracting the features from the convolutional kernels and compares them to traditional approaches. In chapter 7 the results are revised and items for further investigation and optimization are presented together with a more general outlook on the topic of analyzing Neural Networks to gain insights into problems and not just as solutions to them.

# Chapter 2

## Dataset

The Lung Image Database Consortium image collection (LIDC-IDRI) is a publicly available dataset that was generated through the joined effort of seven academic centers and eight medical imaging companies and that contains 1018 cases. It consists of diagnostic and lung cancer screening thoracic computed tomography (CT) scans with marked-up annotated lesions. More information to the origin of the dataset can be found in the appendix B.1 and the referenced paper by Armato [AMB<sup>+</sup>11]. The following sections provide an overview of the data structure and the implemented preprocessing.

### 2.1 Content and Structure

The dataset contains a folder for each patient. These folders contain a full chest CT scan and the annotations by the radiologists. The CT scan data is encoded in a list of DICOM (Digital Imaging and Communications in Medicine) files and the annotations as one XML (extended markup language) file. The structure of both file types is described in the upcoming sections. More details on how the dataset was formed and how the images are generated by the scanners as well as the parameters that play into that can be found in the appendix B and B.3.

#### 2.1.1 Scan Data Structure

DICOM is a file format for storing medical images with for the use case relevant meta information. It is not only used for CT scans but also for radiography, ultrasonography and MRI data. It was initially introduced by the American College of Radiology (ACR) and National Electrical Manufacturers Association (NEMA) under the name ACR/NEMA 300 in 1985, but further redefined and finally in the third version released under the name DICOM in 1993 [Pia08].

The cases that scans are provided for in the dataset fulfill certain criteria. The CT scans are exclusively of the lung and do not contain other body parts or organs. The reconstruction interval and collimation are kept at  $< 3\text{mm}$ . This means that there are differences in the resolution of the scan data (naturally through the different equipment used during recording), but that it is limited with an upper bound. Still one can find patients with 124 – 529 recorded images in the data. The scan data may also include noise or other disruptive factors like metal

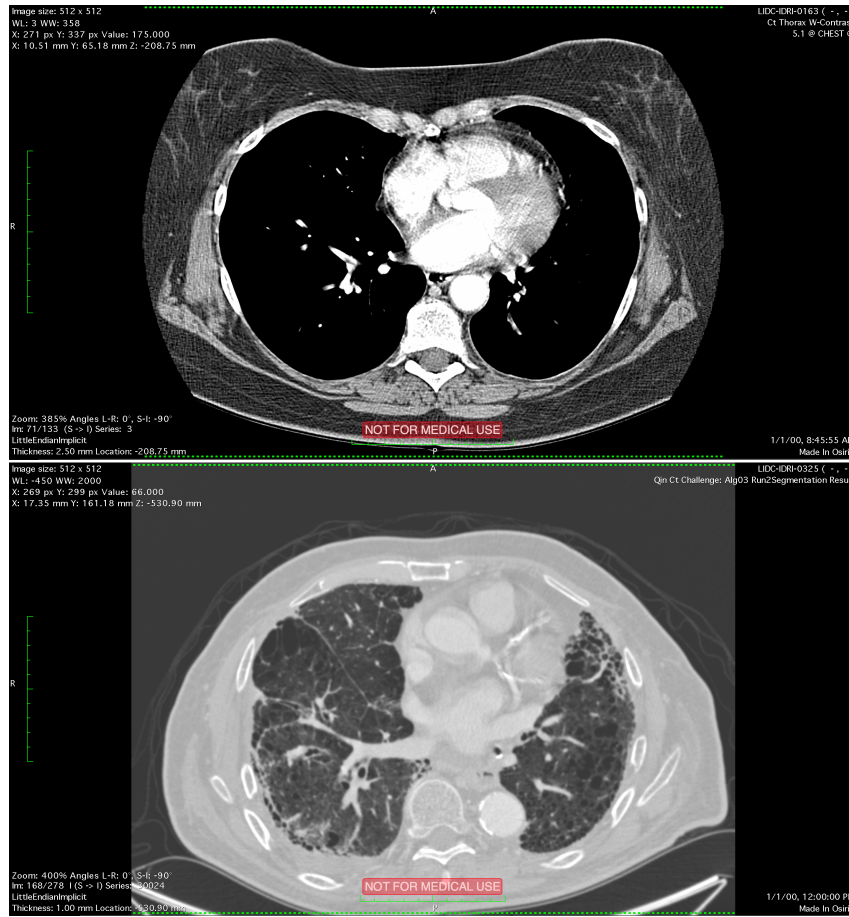


**Figure 2.1:** Two slices from different patients in the dataset. Images have been generated with OsiriX Lite [RSR04]. The information in the corner of the picture is extracted from the meta information stored in the DICOM format.

(heart pacers e.g.) as well as other pathological features as long as those do not interfere with the visibility of the nodules in a drastic sense.

The included cases have between 0 and 6 nodules with a longest diameter between 3 – 30 mm. The term nodule refers to a broad spectrum of tissue abnormalities and can represent not only lung cancer but also other metastatic diseases or non-cancerous processes or lesions that have a nodular morphology. Typical slices from the data can be seen in Figure 2.1.

The additional information about the patients that is usually stored with the scans (like age, name, gender) are anonymized in this dataset.

### 2.1.2 Annotation Structure

Two different types of nodules are encoded in the data: nodules with a diameter of  $\geq 3$  mm and nodules smaller than that. The big nodules have extensive information stored with them: a rich edge map which outlines a complete contour for them in all sections (as seen in Figure 2.2)

---

```

<noduleID>IL057_127581</noduleID>
<characteristics>
    <subtlety>4</subtlety>
    <malignancy>3</malignancy>
    [...]
</characteristics>

<edgeMap>
    <xCoord>103</xCoord>
    <yCoord>391</yCoord>
</edgeMap>

<imageZposition>-232.535004</imageZposition>

<edgeMap>
    <xCoord>104</xCoord>
    <yCoord>393</yCoord>
</edgeMap>

```

**Figure 2.2:** A shortened example XML annotation for a nodule with diameter  $\geq 3\text{mm}$ .

and a measure for their characteristics (like their subtlety and malignancy on a scale from 1 to 5). Those extra information have not been used in the learning process for this thesis, but enable research on further classification and localization tasks.

Nodules with a smaller diameter have less information stored with them. They only contain the approximate center of mass for the nodule as seen in Figure 2.3.

```

<noduleID>7</noduleID>
<roi>
<imageZposition>-227.535004</imageZposition>
<imageSOP_UID>1.3.6.1.4...</imageSOP_UID>
<inclusion>TRUE</inclusion>
<edgeMap>
    <xCoord>127</xCoord>
    <yCoord>370</yCoord>
</edgeMap>
</roi>

```

**Figure 2.3:** Nodules with a diameter of  $< 3\text{mm}$  have only the center of mass stored.

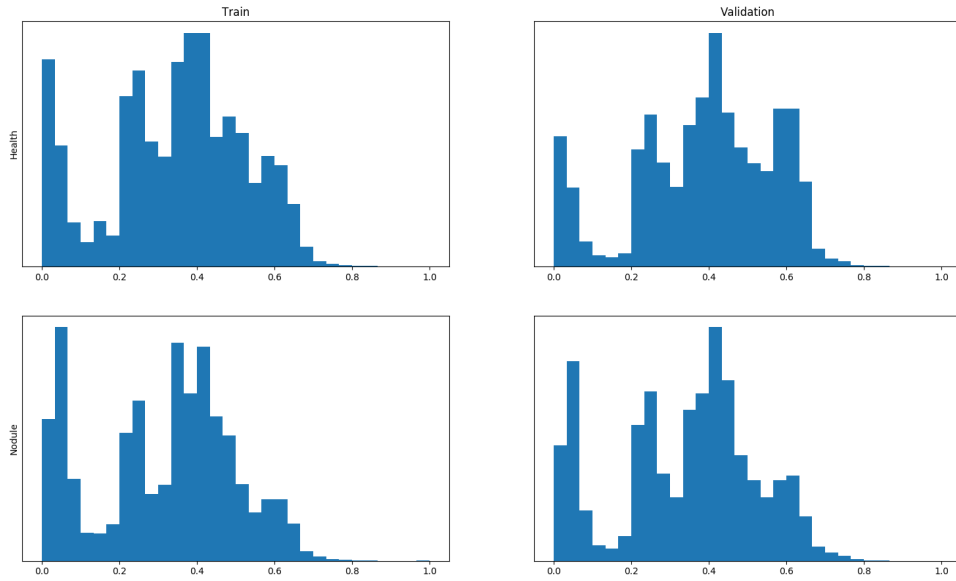


**Figure 2.4:** Distribution of the normalized pixel values for both classes in the training and validation set (1000 instances per set). This data is used for learning the network.

## 2.2 Preprocessing

The data is available in the form of sub-folders for each patient that contain the CT scan results in DICOM file format and the annotation data as XML files. The following sections describe the read in and slicing of the data.

### 2.2.1 Reading in the data

The whole dataset was randomly distributed to 3 folders in a 60 : 20 : 20 split ratio: train, validation and test. The training dataset is used during the learning process of the neural network. The validation dataset is used to measure the performance of the network while it is trained on the train dataset. See Figure 2.4 for a distribution of values for the two classes.

Each of the folders contains a list of patients containing one or more sub-folders with CT scans. Some of the extra folders for a patient contain only a few scans and not a complete CT. Those folders were ignored. With the use of the Python package dicom [Mas11] the CT scans are converted to a 3 dimensional array. The annotation XML files are evaluated to find the location of the nodules. In the case of nodules with a diameter of < 3mm the center of mass value is used, for the bigger nodules that have information of the whole edgemap, the mean over all dimensions is used as an approximation for the center of mass of those nodules. 147 patient files contained no real nodules or had corrupted data (the XML file had a corrupted structure or wrong formatting that prevented the algorithm from extracting the nodule coordinates, one file

had a slice thickness of 0 e.g.). Those files have as well been excluded for the learning process.

### 2.2.2 Slicing the patches

The information from the annotations is used to generate the patches from the complete scan. A fixed number of patches is generated from the data per patient. The patches for the healthy data are cut randomly from the tissue that contain no nodules while the patches with the nodule information are randomly picked around the nodule's center. Determining the center of a nodule is easy in the cases of the nodules with  $< 3\text{mm}$  diameter. The resulting shape of the patches is (50, 50, 5). It makes sense to take less value in the z direction since the resolution of the CT scans is lower in that direction (more information about the scanners can be found in the appendix B.3).

# Chapter 3

## Current Approaches

This chapter illustrates the current state of the art in the field of automated nodule detection. Roughly the field can be divided among the used methods in the *classical* approaches and the deep learning approaches. It also describes how this thesis is situated in the field and what is done differently compared to previous papers.

### 3.1 Classical Approaches

Nodule detection is a complex and potentially life-saving task, so it makes sense that there is a scientific community dedicated to finding algorithmic approaches to aid the radiologists. In this section some of the published papers in this domain and the techniques they use will be explained. In principal algorithms applied to the lung CT images can be subdivided in several stages (as can be for example seen in 3.1). Similar to other computer vision algorithms those can be roughly clustered in the following: Segmentation, Candidate Selection, Classification.

#### 3.1.1 Segmentation

A lung CT scan contains more anatomical structure than just the lung area. It is necessary to exclude the trachea, heart as well as the spine from the slices in order to solely focus on the lung tissue. Armato et al. [AGM<sup>+</sup>99, AGM01] use for example twice a gray-value thresholding. First with a fixed parameter to exclude the background (the air surrounding the patient) and a second time with a varying threshold based on the distribution of gray values in the slice. Roughly two peaks mark the heart and the more solid surrounding tissue (which result in brighter values on the scan image) and a lower peak for the darker region - the threshold is then chosen between the two peaks. Gurcan et al. [GSP<sup>+</sup>02] use k-means clustering (with  $k = 2$ ) on the histogram to separate the two groups.

Juxtapleural nodules can pose a problem in this scenario since they lie closely connected to the membrane (pleura) that lines the lung and might be erroneously excluded. They produce cavities on the initially segmented lung and need to be corrected. A rolling ball filter can be used to smooth the contures of the lung again and rightly add the juxtapleural nodules to the inner lung region [AGM<sup>+</sup>99]. Another approach, used by Gurcan et al. [GSP<sup>+</sup>02] is comparing the distance between two points measured along the contour that was formed by

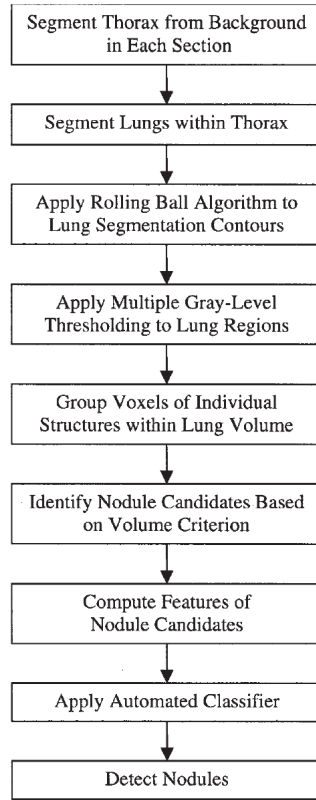


**Figure 3.1:** This image is taken from Armato's paper “Computerized Detection of Pulmonary Nodules on CT Scans” [AGM<sup>+</sup>99] and describes on one specific example how a traditional approach towards nodule detection is modeled.

the initial segmentation and comparing it to the euclidean distance between the points. If the ratio is bigger than a preselected threshold the points are again connected with a line. The final segmentation in the end looks similar to Figure 3.2.

### 3.1.2 Candidate Selection

From the segmented lung region nodule candidates are selected. This selection can be done either by intensity- or model-based methods. The following text describes exemplary one method for each of the two types of algorithms and highlights concerns or limits of those. Armato et al. [AGM<sup>+</sup>99] use a multiple thresholding of the slices to obtain a set of 15 CT scans that only contain pixels above an increasing threshold. Now the 10 neighborhood of all on-pixels is used to group pixels together in structures, which are then classified by their volume. All structures that have a volume less than  $14.1\text{cm}^3$  are nodule candidates and the others are disregarded.

Another approach involves using a predefined geometrical model to find the nodule candidates. Ye et al. [YLD<sup>+</sup>09] use for example a shape index as defined in Equation 3.1 (this index is basically just a rescaled version of the original shape index that produces values between  $-1, 1$

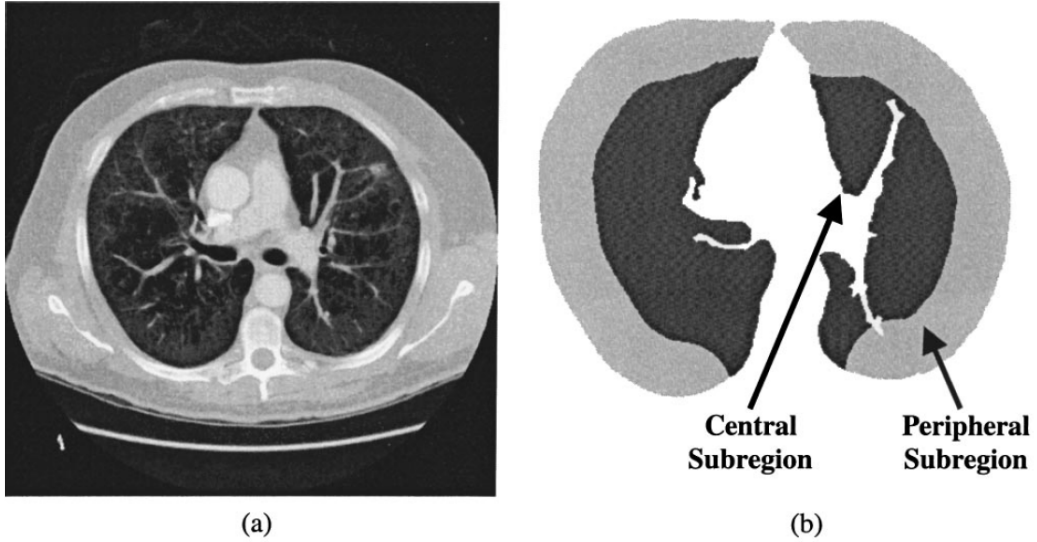


**Figure 3.2:** This image is taken from Gurcan's paper "Lung nodule detection on thoracic computed tomography images: Preliminary evaluation of a computer-aided diagnosis system" [GSP<sup>+</sup>02] and shows the result of the segmentation process.

to 0, 1) to classify candidates based on the shape of their surface.  $k(p)$  are the values of the principal curvature in a point of interest  $p$ . Nodules obtain a higher score (closer to 1) compared to blood vessels, which have a prolonged shape.

$$SI(p) = \frac{1}{2} - \frac{1}{\pi} \arctan \frac{k_1(p) + k_2(p)}{k_1(p) - k_2(p)} \quad (3.1)$$

Using sphericity as a strong nodule indicator may lead to a model that is highly sensitive to only one type of nodules while ignoring nodules that lie close to the chest wall and are not perfectly round or GGO nodules that are more diffuse in their morphology. Model-based algorithms on the other hand have the advantage of being able to incorporate a priori knowledge more easily. Different model parameters for example can be fine tuned due to the vessel density in a region of the lung - e.g. blood vessels are more common in the central region of the lung. The extracted nodule candidates can now be further processed in the classification step.

### 3.1.3 Classification

The candidates have to be classified to separate nodules between cancerous and non-malicious types. The classification itself can again be split into several steps, but this section will only highlight a few examples to give an overview. Armato et al. [AGM<sup>+</sup>99] and Gurcan et al. [GSP<sup>+</sup>02] use a linear discriminant analysis classifier along several nodule features like volume, sphericity, radius of equivalent sphere and more to separate real nodules from other structures which have been found by the before described selection process. Firmino et.al [FMM<sup>+</sup>14] provide a very rich comparison of different CAD methods and their performance, which can be seen in

Figure 3.3.

**Table 2 Performance comparison of lung nodule detection methods by sensitivity, FP, number of nodules, size and response time**

| Methods                        | Year | Sensitivity | FP            | N° of nodules | Size              | Response time | Type of nodules  |
|--------------------------------|------|-------------|---------------|---------------|-------------------|---------------|--|
| Xu et al. [70]                 | 1997 | 70%         | 1,7 per image | 122           | 4 - 27mm          | 20s           | NI   |
| Armatto et al. [48]            | 1999 | 70%         | 9,6 per case  | 187           | 3,1 - 27,8mm      | NI            | Solitary and juxtapleural                                      |
| Lee et al. [45]                | 2001 | 72%         | 25,3 per case | 98            | < 10mm            | 187 min       | NI   |
| Suzuki et al. [71]             | 2003 | 80,3%       | 4,8 per case  | 121           | 4 - 27mm          | 1,4s          | Juxtavascular, hilum, ground-glass opacity and juxtapleural    |
| Murphy et al. [40]             | 2007 | 84%         | 8,2 per case  | 268           | 2 - 14mm          | NI            | Pleural and non-pleurral                                       |
| Ye et al. [23]                 | 2009 | 90,2%       | 8,2 per case  | 220           | 2 - 20mm          | 2,5 min       | Juxtavascular, isolated, ground-glass opacity and juxtapleural |
| Messay, Hardie and Rogers [21] | 2010 | 82,66%      | 3 per case    | 143           | 3 - 30mm          | 2,3 min       | Juxtavascular, solitary, ground-glass opacity and juxtapleural |
| Liu et al. [20]                | 2010 | 97%         | 4,3 per case  | 32            | NI                | NI            | Solitary   |
| Kumar et al. [75]              | 2011 | 86%         | 2,17 per case | 538           | NI                | NI            | NI   |
| Tan et al. [76]                | 2011 | 87,5%       | 4 per case    | 574           | 3 - 30mm          | NI            | Isolated, juxtavascular, and juxtapleural                      |
| Hong, Li and Yang [22]         | 2012 | 89,47%      | 11,9 per case | 44            | NI                | NI            | Solitary   |
| Cascio et al. [65]             | 2012 | 97%         | 6,1 per case  | 148           | $\geq 3\text{mm}$ | 1,5 min       | Internal and juxtapleural                                      |
| Orozco et al. [63]             | 2012 | 96,15%      | 2 per case    | 50            | NI                | NI            | NI   |
| Teramoto and Fujita [24]       | 2013 | 80%         | 4,2 per case  | 103           | 5 - 20mm          | 30s           | Juxtavascular, isolated, ground-glass opacity and juxtapleural |

(NI = Not Informed).

**Figure 3.3:** This table is taken from Firmino et.al’s paper “Computer-aided detection system for lung cancer in computed tomography scans: Review and future prospects” [FMM<sup>+</sup>14] and shows the performance of different algorithms. It is noticeable how the number nodules used for training differ widely between the cases.

## 3.2 Deep Learning Approaches

A deep learning approach as defined for this thesis is any approach that utilizes in at least one of the above explained steps a neural network with more than 2 layers. All of the found papers use a mixed strategy: using more classical candidate selection strategys and using the neural network only in the final classification step. Only two other papers use 3D Convolutional Neural Networks: Anirudh et al. [ATBK16] and Huang et al. [HSV17].

## 3.3 This Thesis

Where can this thesis be positioned in the field of Lung CT analysis and nodule detection? Given the sections above it is clear that it is part of the deep learning approaches, but differs in the sense that no prior candidate selection is performed on the data. The classification is based on raw ct scan patches that are fed to the network as is. The amount of data used for the training process also differs compared to the more classical papers. 2565 nodule and healthy patches have been used for the classification.

This means that no further features of the nodule can be determined like there malignancy score for example.

# Chapter 4

## Methods

The following sections highlight the used methods and give a rough overview about the used tools. First the used environment of software tools is described. Then the theoretical concept of a Convolutional Neural Network is explained and how it was trained on the available resources. A more extensive explanation to the different software packages and computational resources can be found in the appendix A.

### 4.1 Software Packages

Writing a program for solving the task of nodule detection with neural networks makes the use of certain frameworks necessary. Using Python as a versatile programming language allowed for writing code for all aspects of the project: from data preprocessing and training the network to analyzing the results. The language narrows down the number of frameworks available for training neural networks. For this thesis Tensorflow (A.3) was chosen since it is at the moment the most active framework (in the sense of implementation Figure 5.1). Other frameworks like Cafe, Theano and Keras would have been valid choices as well. The Sun Grid Engine of the institute is used for automated execution on several machines (see A.2 for details) and was used for training the model.

### 4.2 Convolutional Neural Network

In this thesis a 3D Convolutional Neural Network (CNN) is used to classify the CT slices. The main motivation to use a 3D CNN in the case of nodule detection are the morphological features of the nodules that could not be fully utilized by a convolution that is only applied to 2D sections of the nodule. A CNN is similar to other artificial neural networks (ANNs) in the sense that it only uses forward connections, has an input and output layer and an arbitrary number of hidden layers in between. The hidden layers in a convolutional network are either convolutional or pooling layers which are in the end followed by one or more dense layers that perform the classification. Each of those layers is described in more detail in the following sections.

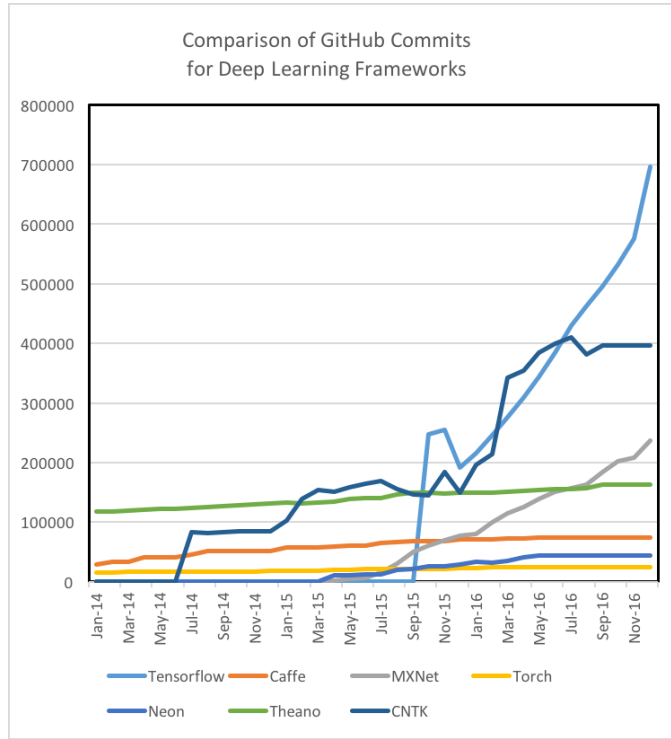


**Figure 4.1:** Number of commits for the different deep learning frameworks. This figure is taken from Shapiro [PS17].

#### 4.2.1 Convolutional Layer

The convolutional layer consists of  $1..n$  kernels that are represented through shared weights that compared to classic convolution in computer vision do not *slide* across the input but are duplicated across the image in the defined distance (called stride). For this CNN 3 convolutional layers were used with 40, 20 and 20 kernels each. The convolution takes place in 3D which means that the filter kernels are also 3 dimensional and the stride is as well defined in all 3 directions of the input image ( $x, y, z$ ). The kernel size was chosen to be  $(3 \times 3 \times 3)$  in accordance with Huang et al.'s [HSV17] implementation for nodule classification.

As the layers of convolution stack the extracted features from the first layer are combined to more complex shapes. The layers contain also a batchnormalization step as described in [IS15] that was implemented in the Tensorflow layers class. Batchnormalization is scaling the activation of the layer to become normally distributed in each dimension of the features, but has additional parameters that can be learned to shift and scale these values again. This should bring several advantages like: reducing the dependence of the initialization method and allowing for higher learning rates. The batchnormalization is followed by a max pooling layer which is applying a max-filter of size  $(2, 2, 2)$  to the normalized activations.

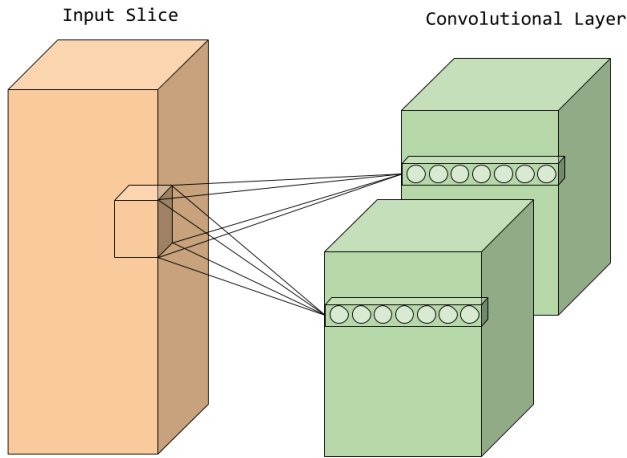


**Figure 4.2:** Structure of a convolutional layer. In image analysis the third dimension may encode the color informational, but in the example of Lung CT data it encodes additional spatial information. The figure shows two separate kernels that have shared weights for each kernel position in the input.

#### 4.2.2 Dense Layers

The activations from the last convolutional layer are flattened into a  $(1 \times n)$  vector and fed to the neurons of the fully connected layer. The network has two dense layers with 64 neurons each. The activation function of the rectified linear unit is a simple maximum of the weighted inputs. The combined complete structure of the network can be seen in Figure 5.3.

### 4.3 Training

The input to the network are the slices that have been the result of the before described pre-processing and are fed to the network in batches. They are augmented by randomly flipping them in x and y plane (examples can be seen in 5.4). The augmentation is applied to make the learned classification more robust against distortions in the input. It makes sense in this specific scenario since the nodules are growing in different shapes and locations in the lung and flipping them is not producing an impossible input to the network.

Regularization methods used for this network include batchnormalization and dropout. Batchnormalizaton is in TensorFlow implemented as described by Ioffe and Szegedy [IS15] and has been described already in section 5.2.1. Dropout is another regularization method that was used in this thesis. It basically means that during training random neurons of the network are dropped - training effectively several models at once, as discovered by Srivastava et al. [SHK<sup>+</sup>14], which should increase the overall performance of the network. During training no improved performance could be observed when applying dropout throughout the whole network.

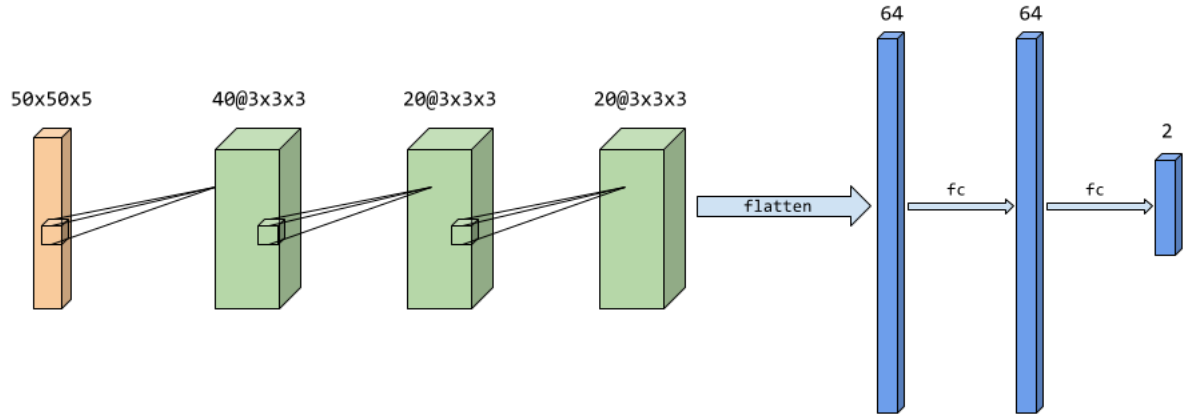


**Figure 4.3:** Architecture of the neural network. Each of the convolutional layers is composed of a 3D convolution layer with the respective filter size followed by a batch normalization and a pooling layer. The pool size is (2, 2, 2) with a stride of (1, 1, 1). The structure of the neural network resembles the one described by Huang [HSV17].

It was rather harmful if applied to the convolutional layers. The final model uses dropout only in the fully connected layers.

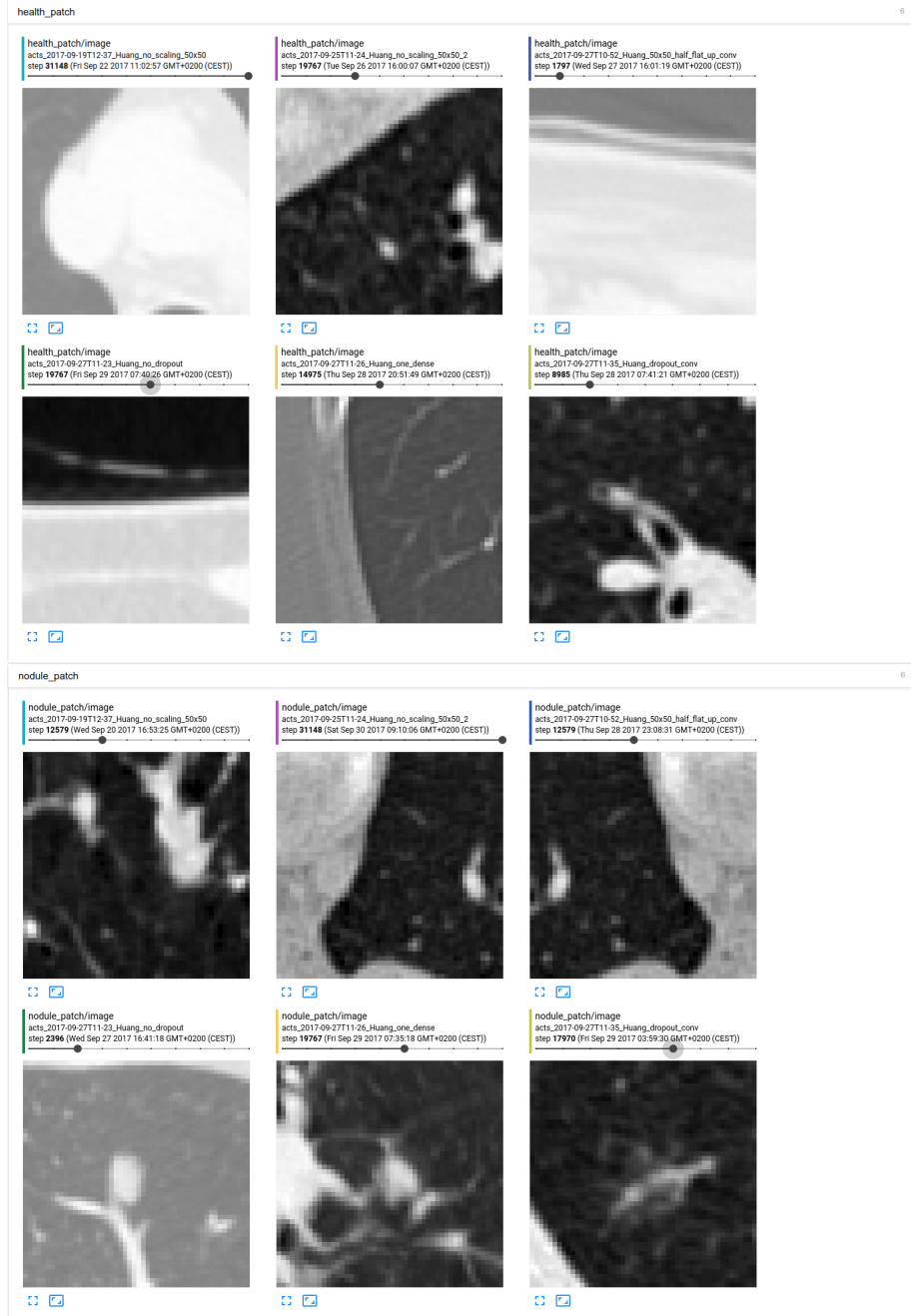


**Figure 4.4:** Input data for the cases of healthy and nodule patches. The image is taken from Tensorboard and shows in the case of nodules the random permutation of the input data.

# Chapter 5

## Methods

The following sections highlight the used methods and give a rough overview about the used tools. First the used environment of software tools is described. Then the theoretical concept of a Convolutional Neural Network is explained and how it was trained on the available resources. A more extensive explanation to the different software packages and computational resources can be found in the appendix A.

### 5.1 Software Packages

Writing a program for solving the task of nodule detection with neural networks makes the use of certain frameworks necessary. Using Python as a versatile programming language allowed for writing code for all aspects of the project: from data preprocessing and training the network to analyzing the results. The language narrows down the number of frameworks available for training neural networks. For this thesis Tensorflow (A.3) was chosen since it is at the moment the most active framework (in the sense of implementation Figure 5.1). Other frameworks like Cafe, Theano and Keras would have been valid choices as well. The Sun Grid Engine of the institute is used for automated execution on several machines (see A.2 for details) and was used for training the model.

### 5.2 Convolutional Neural Network

In this thesis a 3D Convolutional Neural Network (CNN) is used to classify the CT slices. The main motivation to use a 3D CNN in the case of nodule detection are the morphological features of the nodules that could not be fully utilized by a convolution that is only applied to 2D sections of the nodule. A CNN is similar to other artificial neural networks (ANNs) in the sense that it only uses forward connections, has an input and output layer and an arbitrary number of hidden layers in between. The hidden layers in a convolutional network are either convolutional or pooling layers which are in the end followed by one or more dense layers that perform the classification. Each of those layers is described in more detail in the following sections.

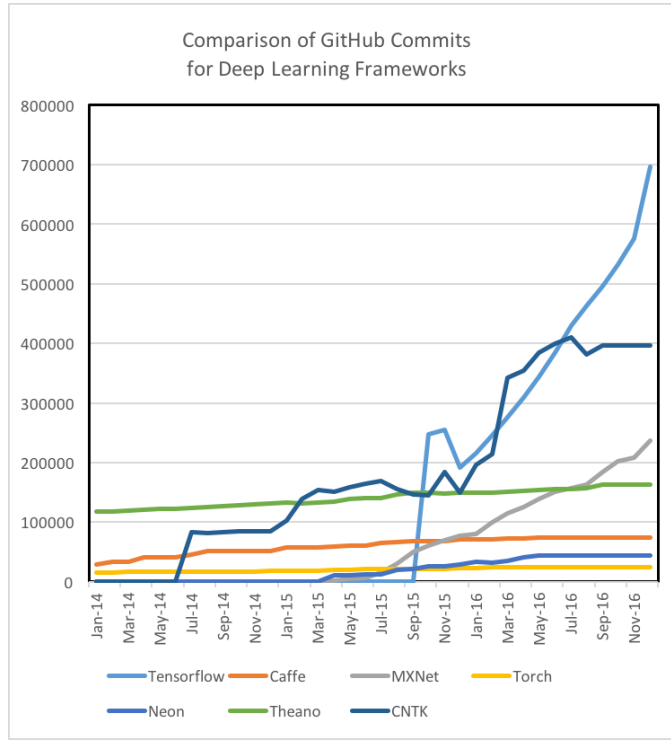


**Figure 5.1:** Number of commits for the different deep learning frameworks. This figure is taken from Shapiro [PS17].

### 5.2.1 Convolutional Layer

The convolutional layer consists of  $1..n$  kernels that are represented through shared weights that compared to classic convolution in computer vision do not *slide* across the input but are duplicated across the image in the defined distance (called stride). For this CNN 3 convolutional layers were used with 40, 20 and 20 kernels each. The convolution takes place in 3D which means that the filter kernels are also 3 dimensional and the stride is as well defined in all 3 directions of the input image ( $x, y, z$ ). The kernel size was chosen to be  $(3 \times 3 \times 3)$  in accordance with Huang et al.'s [HSV17] implementation for nodule classification.

As the layers of convolution stack the extracted features from the first layer are combined to more complex shapes. The layers contain also a batchnormalization step as described in [IS15] that was implemented in the Tensorflow layers class. Batchnormalization is scaling the activation of the layer to become normally distributed in each dimension of the features, but has additional parameters that can be learned to shift and scale these values again. This should bring several advantages like: reducing the dependence of the initialization method and allowing for higher learning rates. The batchnormalization is followed by a max pooling layer which is applying a max-filter of size  $(2, 2, 2)$  to the normalized activations.

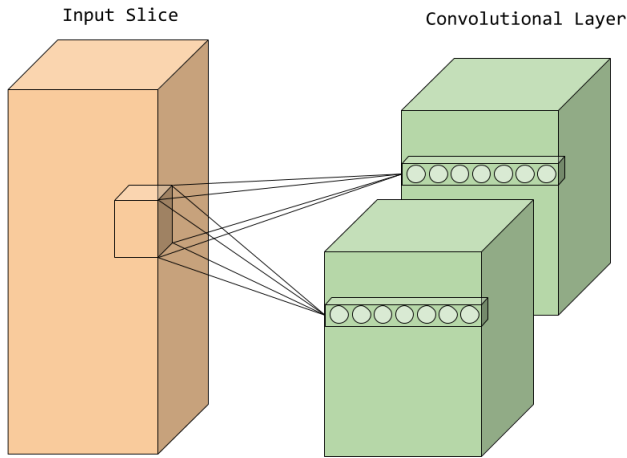


**Figure 5.2:** Structure of a convolutional layer. In image analysis the third dimension may encode the color informational, but in the example of Lung CT data it encodes additional spatial information. The figure shows two separate kernels that have shared weights for each kernel position in the input.

### 5.2.2 Dense Layers

The activations from the last convolutional layer are flattened into a  $(1 \times n)$  vector and fed to the neurons of the fully connected layer. The network has two dense layers with 64 neurons each. The activation function of the rectified linear unit is a simple maximum of the weighted inputs. The combined complete structure of the network can be seen in Figure 5.3.

## 5.3 Training

The input to the network are the slices that have been the result of the before described pre-processing and are fed to the network in batches. They are augmented by randomly flipping them in x and y plane (examples can be seen in 5.4). The augmentation is applied to make the learned classification more robust against distortions in the input. It makes sense in this specific scenario since the nodules are growing in different shapes and locations in the lung and flipping them is not producing an impossible input to the network.

Regularization methods used for this network include batchnormalization and dropout. Batchnormalizaton is in TensorFlow implemented as described by Ioffe and Szegedy [IS15] and has been described already in section 5.2.1. Dropout is another regularization method that was used in this thesis. It basically means that during training random neurons of the network are dropped - training effectively several models at once, as discovered by Srivastava et al. [SHK<sup>+</sup>14], which should increase the overall performance of the network. During training no improved performance could be observed when applying dropout throughout the whole network.

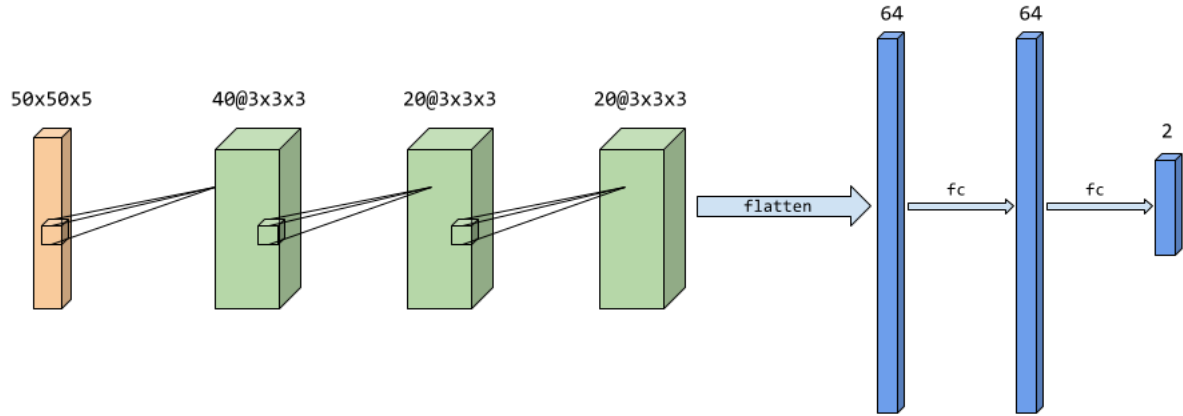


**Figure 5.3:** Architecture of the neural network. Each of the convolutional layers is composed of a 3D convolution layer with the respective filter size followed by a batch normalization and a pooling layer. The pool size is (2, 2, 2) with a stride of (1, 1, 1). The structure of the neural network resembles the one described by Huang [HSV17].

It was rather harmful if applied to the convolutional layers. The final model uses dropout only in the fully connected layers.

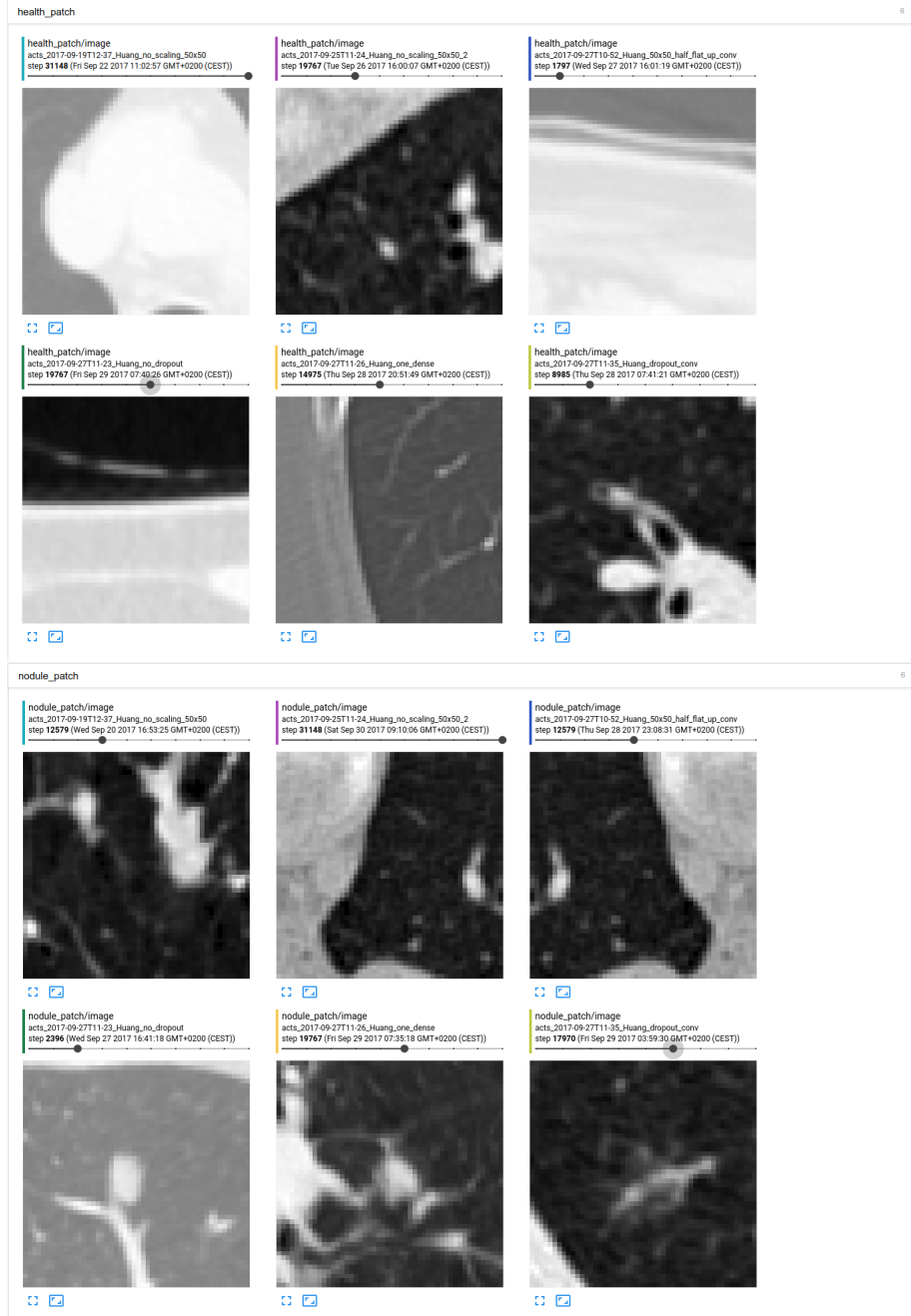


**Figure 5.4:** Input data for the cases of healthy and nodule patches. The image is taken from Tensorboard and shows in the case of nodules the random permutation of the input data.

# Chapter 6

## Results

This chapter presents the result of the training process. The final network performances are evaluated and compared to other papers. The network's extracted features are further analyzed and a way forward is sketched.

### 6.1 The trained Network

The used model is inspired by the network presented in [HSV17] and performs with a sensitivity of around 81% on the validation set and a false positive rate of 0.192 per sample. This is already a better result than reported by Xu et al. [XKM<sup>+</sup>97], Armato et al. [AGM<sup>+</sup>99], Lee et al. [LHF<sup>+</sup>01], Suzuki et al. [SAL<sup>+</sup>03] and Teramoto et al. [TF13].

This is of course not the only metric that needs to be compared in order to evaluate the approach. The way the samples have been produced in this thesis differ from the other papers  
what about fp rate? what about applicability? what about time?

todo: explain why that might not be the most relevant perf number

### 6.2 Analyzing the Network

To understand how a network solves the task it makes sense to look at the patterns it's layers are sensitive to. The convolutional layers allow for visual inspection. Focus on the conv layers, what do they look like? Any hint on the geometry they are sensitive to? Activation patterns to synthetic data and patches from the patients.

How is that best understood? 2 Approaches: first mean activation of the filters in each layer per img.

#### 6.2.1 Mean Class Activation

### 6.3 Bridge to other Approaches

How could a comparison at all be achieved? What is hindering the straightforward comparison of the kernel weights? Draw out a method to do that Show what has been done Compare

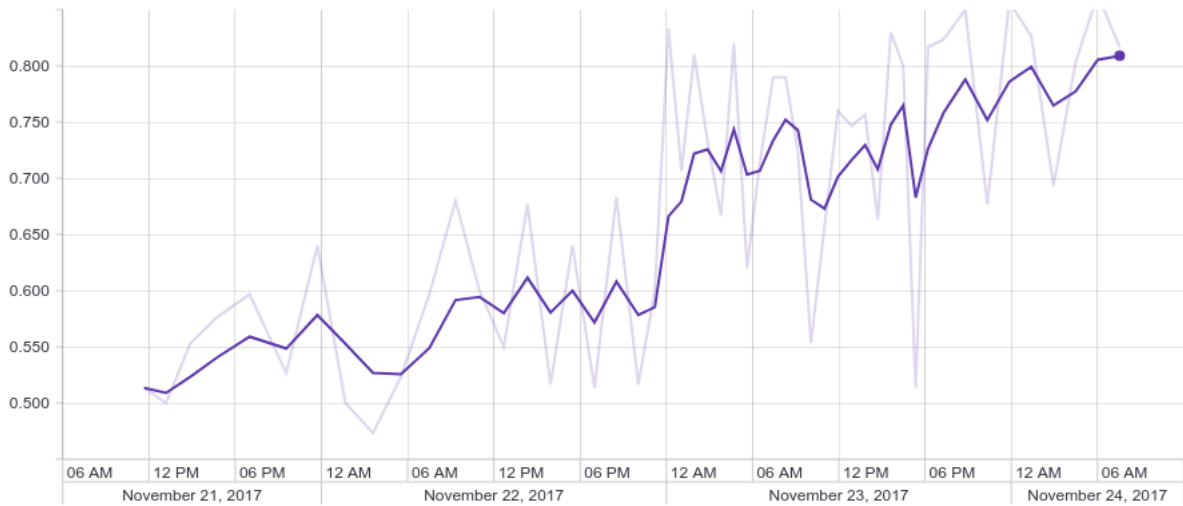


**Figure 6.1:** Learning process of the network - the graph shows the development of the accuracy of the network on the validation set. The darker line represents the smoothed values of the lighter line. Since the training is performed on the CPU (GPU can not be utilized since the network was too big.), it takes several days.

performance to hand crafted approaches, take numbers out of papers  
what could be similar features in the network?

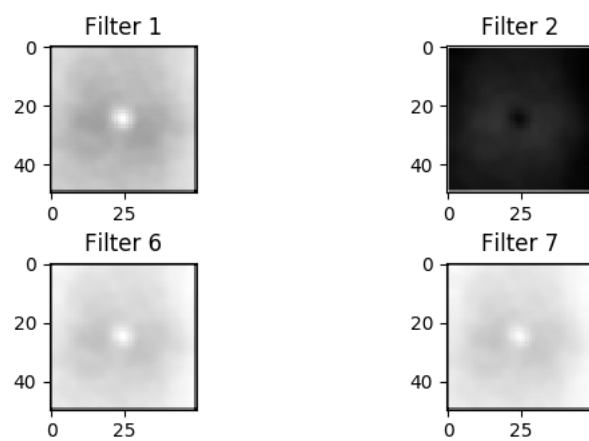


**Figure 6.2:** The mean activation from 500 nodule patches of the validation set. Already in the first layer the receptive field is focusing on the center area, where the nodule resides.

# Chapter 7

## Discussion

This thesis started out with two research questions: First: can a 3D CNN be trained to perform the task of nodule detection and second, how can it's learned features be extracted and used for understanding the solution?

To the first question: it was shown that it is possible to train a network with promising results upon which further optimization could be applied. The performance of the learned network was at XXX % which is surprising for it's simple structure. With more time and computational power it seems very possible to increase the performance further. Ways forward could include more samples from the database and a richer augmentation of the samples which allow for training even deeper networks. Other network parameters could easily be systematically varied and tested for effectiveness, allowing for further optimization.

The code for this thesis is openly available on "<https://github.com/AndreaSuckro/acts>".

Future thought: tumor size estimation to determine growth over time.

Was it really worth doing this task with NNs?

### 7.1 Items of future code optimization

**cluster parameters** are at the moment not completely adapted to the optimal need of the learning process and could be further improved.

**input pipeline** the input pipeline is not using queues as suggested in the TensorFlow documentation, but just reads in all the lung ct data.

**preprocessing** further steps in the preprocessing could improve the results, for example a true 3d rotation and different scales of the same patch could be used. The ratio of healthy and nodule patches is at the moment way to high (50 : 50). This could be adjusted to a more reasonable value although this may prolong the training phase.

**Training time** due to the way the institute set up the grid, all users have a walltime which stops training after several hours. One could pick up the training after being shut down from the latest checkpoint.

## 7.2 Items of future investigation

**Fully convolutional network** to eliminate the influence on the performance of the dense layers and keep the location information until the end.

**Optimizers** it would have been nice to check for the influence of different optimizers for this problem.

**Minimal Architecture** how can the number of layers and/or neurons be reduced. What is the optimal distribution for the filter sizes to be used.

**Metrics of one patient** For one patient it would be interesting to see how the network fairs when one cube after the other is selected and fed in to the network. How does the FP rate look for example?

# **Appendix A**

## **Software**

### **A.1 Python**

Python is a multi-purpose language, which means that no specific coding paradigm is imposed on the user, but one can use scripting as well as object oriented design alike. This allows for a very flexible style of programming which was used in this project for writing little tools that help with the data preprocessing as well as more complex code for the learning pipeline and the analysis of the network. Python is also widely used by the machine learning community which makes it easier to look up code examples and questions on forums like Stackoverflow. The specific version used in this thesis is 3.6 and all used packages are downloaded via pip or conda. The dependencies are listed in the file "act-env.yml" and can be installed with it as well.

### **A.2 Oracle Grid Engine**

Our institute uses the work stations and additional hardware resources in form of a grid computing system that is managed by the Oracle grid engine (formerly known as Sun Grid Engine). The software manages the distribution of jobs to the nodes in the cluster, based on availability and resource requirements. The following bash script A.2 is used in the learning process of the network. It defines the name of the job and the necessary memory that should be available on the machines.

```

#!/bin/bash
#$ -N acts
#$ -l mem=128G
#$ -pe default 8
#$ -j y
#$ -v TESTNAME,WD,LOG_PATH

export LD_LIBRARY_PATH=$HOME/.local/cuda/lib64/:$LD_LIBRARY_PATH
export LIBRARY_PATH=$HOME/.local/cuda/lib64/:$LIBRARY_PATH
export CPATH=$HOME/.local/cuda/include:$CPATH
export PATH="/net/store/cv/projects/software/conda/bin:$PATH"

. activate acts-cpu

python3 $WD/acts/src/learn.py \
    -d /net/store/cv/projects/datasets/image/pub/LIDC-IDRI/ \
    -l $LOG_PATH \
    -e 2000 \
    -s 1 \
    -b 5 \
    -n $LOG_PATH \
    -t $TESTNAME \
    -p 3000

```

**Listing A.1:** The code for calling the learning script. The parameters in the beginning are the information for the Oracle Grid Engine.

No machine with less memory is considered by the distributor as an execution host for this job. If the memory is set too low for the job, it can not complete the task and fails during execution since no more than the requested memory can be allocated dynamically during run time. It is also defined how many cores should be used on the host machine to run the job in parallel. The job can be directly executed via the command line or with a script (which makes more sense if one plans to run the grid job multiple times). The command used for this operation is *qsub*. Since the grid engine works with a concept of different queues it is possible to submit the job also just to specific queues, where one has the maximum execution time for example.

```

#!/bin/bash
export TESTNAME=Huang_no_scaling_50x50
export LOG_PATH=/net/store/cv/projects/tmp/asuckro/logs/acts_$(date +%Y-%m-%d-%H-%M)
mkdir -p $LOG_PATH
qsub -q all.q -o $LOG_PATH/grid.out runActs.sge

```

**Listing A.2:** The code for submitting the script to the scheduler.

All jobs are only allowed for a specified maximal amount of time depending on the users setting and the queue the job is transmitted to. All outputs to the console are logged in a file that can be specified with the '-o' variable.

### A.3 Tensorflow

Tensorflow is a software library developed by Google Brain that aids the development of machine learning applications by expressing computations as a graph and taking care of the underlying optimization and execution. The version used in this thesis was 1.3.0. The approach of the framework is applicable to many computational tasks apart from neural networks as long as they can be formalized in a graph, but many of the higher level functions in the framework deal with neural networks. Tensorflow is usable via API's for Python, C++, Haskell, Java, Go, and Rust. Third party packages are available for C#, Julia, R, and Scala. Solving a problem with Tensorflow includes roughly two steps: first one needs to define a graph. A graph in Tensorflow is comprised of nodes, which are either variables (called Placeholders) or operations on those. The convolutional neural network in this thesis is defined like this: placeholders have been created for the lung patches that should be learned on, their respective labels and the phase of the learning (a boolean used for batchnormalization). Those are fed into basic transformation functions that handle the randomized flipping and rotating. The output of this function is fed into some summaries and further piped through the network. The covolutional layers have been scoped and encapsulated to own functions. The result of the dense layers is used to calculate the error that is used for the backpropagation learning in combination with the gradients. The complete structure can be seen in Figure B.1. The completed graph can now be executed in a Tensorflow session. In the session the placeholders are filled with data and a loop is used train the network for a specified number of epochs. Tensorflow only calculates the graph up to the point necessary for the queried parameter. So one can easily just ask for the prediction and skip the weight adaptation step as necessary for the analysis.

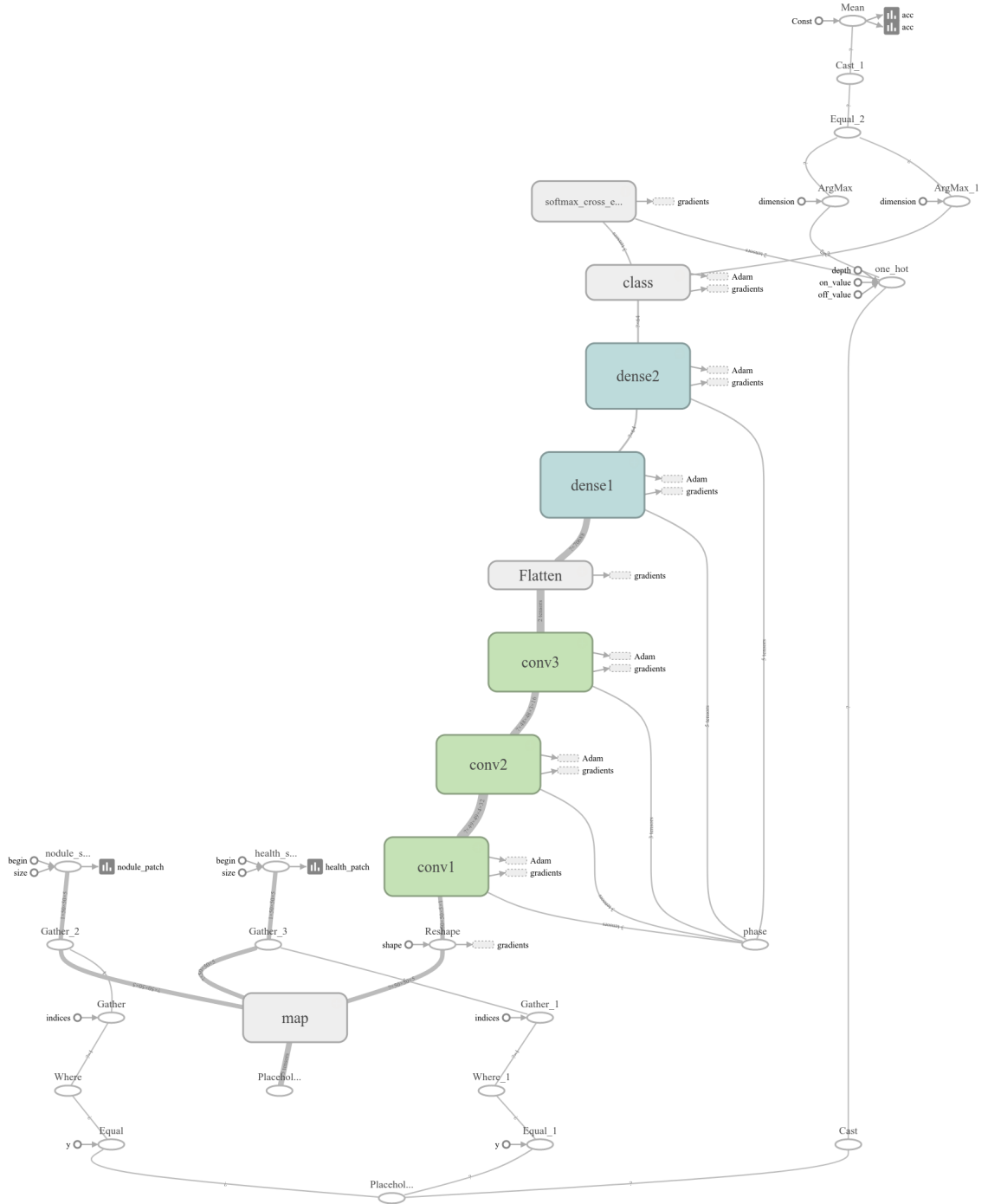


**Figure A.1:** The graph of the model that was generated for this thesis. Scoping of the different layers help a lot to encapsulate similar behavior. The Placeholders do not only flow through the network but are used to generate summaries and reports.

# **Appendix B**

## **Data**

### **B.1 LIDC-IDRI Dataset**

The database as it is available now is the result of a long process that began in April 2000. The National Cancer Institute (NCI) - the U.S. federal government's principal agency for cancer research and training submitted RFAs to create guidelines of how such a combined reference database could look like. The Lung Image Database Consortium (LIDC) was formed by the Weill Cornell Medical College, University of California, Los Angeles, University of Chicago, University of Iowa and University of Michigan in 2001. There task was to develop a web-accessible resource for CT scans with attached meta information (like the slice thickness, tube current and other technical specifications as well as patient information) and nodule information based on expert knowledge. The initiative was further advanced in 2004 by the Foundation for the National Institutes of Health (FNIH) which founded the Image Database Resource Initiative (IDRI). They brought two additional medical centers (MD Anderson Cancer Center and Memorial Sloan-Kettering Cancer Center) and eight imaging companies (AGFA Healthcare, Carestream Health, Inc., Fuji Photo Film Co., GE Healthcare, iCAD, Inc., Philips Healthcare, Riverain Medical, and Siemens Medical Solutions) to the initiative. The new members contributed significantly to the whole database and since the process of data aquisition and annotation was streamlined to the previous recorded data the whole set is referred to as the LIDC-IDRI Database. It's aim is to further develop, improve and evaluate automated methods for lung cancer detection and diagnosis and it is comparable to other public datasets in the medical data community like the Digital Database for Screening Mammography (DDSM) which contains roughly 3000 mammograms - a pioneer in the field of public medical imaging datasets.

### **B.2 CT Scanner Technology**

CT scanners cover a wide range of computed tomography devices, like positron emission tomography (PET) and single-photon emission computed tomography (SPECT), but most commonly refer to tube X-ray scanners. Those scanners work roughly like this: the object of interest (the patient) is placed in the center of the tube. A X-ray emitter rotates around the object and gives off radiation that pierces through the object and is reflected depending on the density of

the materials the object is composed of. Those differences in X-ray absorption make it possible to separate bones from nodules from blood vessels later on in the analysis. The recorded 2D images are combined to a 3D representation, which makes it often necessary that the patients hold very still, even holding their breath during a scanning session.

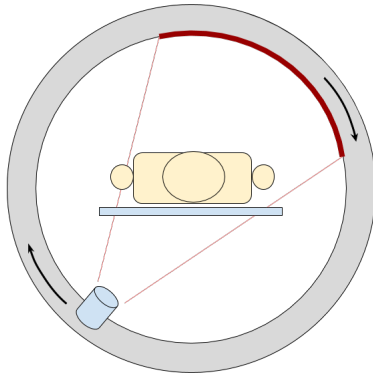


**Figure B.1:** This sketch illustrates the fundamental operation of a CT scanner. An emitter is rotating together with the sensor around the patient's body. The so recorded 2D images are used to reconstruct a 3D representation of the inner body.

### B.3 CT Specifications

A range of scanner manufacturers and models was used to generate the data. The models and the number of samples they provided in the database are listed in the following table:

| GE Medical Systems<br>LightSpeed | Philips Brilliance | Siemens Definition,<br>Emotion, Sensation | Toshiba Aquilion |
|----------------------------------|--------------------|---|------------------|
| 670                              | 74                 | 205                                       | 69               |

**Table B.1:** The distribution of the 1018 samples among each CT scanner model. Values are taken from [AMB<sup>+11</sup>]

The tube peak potential energies used for scan acquisition were as follows: 120 kVp , 130 kVp , 135 kVp and 140 kVp. Tube current ranged from 40 to 627 mA (mean: 222.1 mA).

The number of images per patient depend on the body size but also on the slice thickness which was 0.6 mm, 0.75 mm, 0.9 mm, 1.0 mm, 1.25 mm, 1.5 mm, 2.0 mm, 2.5 mm, 3.0 mm, 4.0 mm and 5.0 mm and the reconstruction interval that ranged from 0.45 to 5.0 mm (mean: 1.74 mm) [AMB<sup>+11</sup>].

The number of pixels for each scan slice depends on the in plane resolution which ranged from 0.461 to 0.977 mm per pixel(mean: 0.688 mm). While the convolution kernels used for

image reconstruction differ among manufacturers, these convolution kernels may be classified broadly as “soft” (67) math formula, “standard/nonenhancing” ( $n=560$ ), “slightly enhancing” ( $n=264$ ), and “overenhancing” ( $n=127$ ) (in order of increasing spatial frequencies accentuated by each class).

# List of Figures

|     |  |    |
|-----|--|----|
| 1.1 | International comparison of age-standardized incidence and mortality rates for lung cancer in the year 2012 . . . . .  | 6  |
| 1.2 | Screenshot of the analyzing software OsiriX. It is the most widely used software in the domain of medical image viewers and offers a free trial version that was used for this thesis. . . . .   | 7  |
| 2.1 | Two slices from different patients in the dataset. Images have been generated with OsiriX Lite [RSR04]. The information in the corner of the picture is extracted from the meta information stored in the DICOM format. . . . .  | 10 |
| 2.2 | A shortened example XML annotation for a nodule with diameter $\geq 3\text{mm}$ . . . . .  | 11 |
| 2.3 | Nodules with a diameter of $< 3\text{mm}$ have only the center of mass stored. . . . .   | 11 |
| 2.4 | Distribution of the normalized pixel values for both classes in the training and validation set (1000 instances per set). This data is used for learning the network.  | 12 |
| 3.1 | This image is taken from Armato's paper "Computerized Detection of Pulmonary Nodules on CT Scans" [AGM <sup>+</sup> 99] and describes on one specific example how a traditional approach towards nodule detection is modeled. . . . .  | 15 |
| 3.2 | This image is taken from Gurcan's paper "Lung nodule detection on thoracic computed tomography images: Preliminary evaluation of a computer-aided diagnosis system" [GSP <sup>02</sup> ] and shows the result of the segmentation process. . . . .   | 16 |
| 3.3 | This table is taken from Firmino et.al's paper "Computer-aided detection system for lung cancer in computed tomography scans: Review and future prospects" [FMM <sup>+</sup> 14] and shows the performance of different algorithms. It is noticeable how the number nodules used for training differ widely between the cases. . . . . | 17 |
| 4.1 | Number of commits for the different deep learning frameworks. This figure is taken from Shapiro [PS17]. . . . .  | 19 |
| 4.2 | Structure of a convolutional layer. In image analysis the third dimension may encode the color informational, but in the example of Lung CT data it encodes additional spatial information. The figure shows two separate kernels that have shared weights for each kernel position in the input. . . . .                              | 20 |

|     |   |    |
|-----|---|----|
| 4.3 | Architecture of the neural network. Each of the convolutional layers is composed of a 3D convolution layer with the respective filter size followed by a batchnormalization and a pooling layer. The pool size is (2, 2, 2) with a stride of (1, 1, 1). The structure of the neural network resembles the one described by Huang [HSV17]. | 21 |
| 4.4 | Input data for the cases of healthy and nodule patches. The image is taken from Tensorboard and shows in the case of nodules the random permutation of the input data.  | 22 |
| 5.1 | Number of commits for the different deep learning frameworks. This figure is taken from Shapiro [PS17].   | 24 |
| 5.2 | Structure of a convolutional layer. In image analysis the third dimension may encode the color informational, but in the example of Lung CT data it encodes additional spatial information. The figure shows two separate kernels that have shared weights for each kernel position in the input.   | 25 |
| 5.3 | Architecture of the neural network. Each of the convolutional layers is composed of a 3D convolution layer with the respective filter size followed by a batchnormalization and a pooling layer. The pool size is (2, 2, 2) with a stride of (1, 1, 1). The structure of the neural network resembles the one described by Huang [HSV17]. | 26 |
| 5.4 | Input data for the cases of healthy and nodule patches. The image is taken from Tensorboard and shows in the case of nodules the random permutation of the input data.  | 27 |
| 6.1 | Learning process of the network - the graph shows the developement of the accuracy of the network on the validation set. The darker line represents the smoothed values of the lighter line. Since the training is performed on the CPU (GPU can not be utilized since the network was too big.), it takes several days.                  | 29 |
| 6.2 | The mean activation from 500 nodule patches of the validation set. Already in the first layer the receptive field is focusing on the center area, where the nodule resides.   | 30 |
| A.1 | The graph of the model that was generated for this thesis. Scoping of the different layers help a lot to encapsulate similar behavior. The Placeholders do not only flow through the network but are used to generate summaries and reports.  | IV |
| B.1 | This sketch illustrates the fundamental operation of a CT scanner. An emitter is rotating together with the sensor around the patient's body. The so recorded 2D images are used to reconstruct a 3D representation of the inner body.  | VI |

# List of Algorithms

# Bibliography

- [AGM<sup>+</sup>99] Samuel G Armato, Maryellen L Giger, Catherine J Moran, James T Blackburn, Kunio Doi, and Heber MacMahon. Computerized detection of pulmonary nodules on ct scans 1. *Radiographics*, 19(5):1303–1311, 1999.
- [AGM01] Samuel G Armato, Maryellen L Giger, and Heber MacMahon. Automated detection of lung nodules in ct scans: preliminary results. *Medical physics*, 28(8):1552–1561, 2001.
- [AMB<sup>+</sup>11] Samuel G Armato, Geoffrey McLennan, Luc Bidaut, Michael F McNitt-Gray, Charles R Meyer, Anthony P Reeves, Binsheng Zhao, Denise R Aberle, Claudia I Henschke, Eric A Hoffman, et al. The lung image database consortium (lidc) and image database resource initiative (idri): a completed reference database of lung nodules on ct scans. *Medical physics*, 38(2):915–931, 2011.
- [ATBK16] Rushil Anirudh, Jayaraman J Thiagarajan, Timo Bremer, and Hyojin Kim. Lung nodule detection using 3d convolutional neural networks trained on weakly labeled data. In *Medical Imaging 2016: Computer-Aided Diagnosis*, volume 9785, page 978532. International Society for Optics and Photonics, 2016.
- [CNC<sup>+</sup>16] Jie-Zhi Cheng, Dong Ni, Yi-Hong Chou, Jing Qin, Chui-Mei Tiu, Yeun-Chung Chang, Chiun-Sheng Huang, Dinggang Shen, and Chung-Ming Chen. Computer-aided diagnosis with deep learning architecture: applications to breast lesions in us images and pulmonary nodules in ct scans. *Scientific reports*, 6:24454, 2016.
- [CVS<sup>+</sup>13] Kenneth Clark, Bruce Vendt, Kirk Smith, John Freymann, Justin Kirby, Paul Koppel, Stephen Moore, Stanley Phillips, David Maffitt, Michael Pringle, et al. The cancer imaging archive (tcia): maintaining and operating a public information repository. *Journal of digital imaging*, 26(6):1045–1057, 2013.
- [DVW13] Trafton Drew, Melissa L-H Võ, and Jeremy M Wolfe. The invisible gorilla strikes again sustained inattentional blindness in expert observers. *Psychological science*, page 0956797613479386, 2013.
- [FMM<sup>+</sup>14] Macedo Firmino, Antônio H Morais, Roberto M Mendoça, Marcel R Dantas, Helio R Hekis, and Ricardo Valentim. Computer-aided detection system for lung cancer in computed tomography scans: review and future prospects. *Biomedical engineering online*, 13(1):41, 2014.

- [GSP<sup>+</sup>02] Metin N Gurcan, Berkman Sahiner, Nicholas Petrick, Heang-Ping Chan, Ella A Kazerooni, Philip N Cascade, and Lubomir Hadjiiski. Lung nodule detection on thoracic computed tomography images: Preliminary evaluation of a computer-aided diagnosis system. *Medical Physics*, 29(11):2552–2558, 2002.
- [HHH<sup>+</sup>15] Kai-Lung Hua, Che-Hao Hsu, Shintami Chusnul Hidayati, Wen-Huang Cheng, and Yu-Jen Chen. Computer-aided classification of lung nodules on computed tomography images via deep learning technique. *OncoTargets and therapy*, 8, 2015.
- [HSV17] Xiaojie Huang, Junjie Shan, and Vivek Vaidya. Lung nodule detection in ct using 3d convolutional neural networks. In *Biomedical Imaging (ISBI 2017), 2017 IEEE 14th International Symposium on*, pages 379–383. IEEE, 2017.
- [IS15] Sergey Ioffe and Christian Szegedy. Batch normalization: Accelerating deep network training by reducing internal covariate shift. In *International Conference on Machine Learning*, pages 448–456, 2015.
- [KAK<sup>+</sup>12] R Kakinuma, K Ashizawa, T Kobayashi, A Fukushima, H Hayashi, T Kondo, M Machida, M Matsusako, K Minami, K Oikado, et al. Comparison of sensitivity of lung nodule detection between radiologists and technologists on low-dose ct lung cancer screening images. *The British journal of radiology*, 85(1017):e603–e608, 2012.
- [KSK<sup>+</sup>15] Peter Kaatsch, Claudia Spix, Alexander Katalinic, Stefan Hentschel, Sabine Luttmann, Christa Stegmaier, Sandra Caspritz, Monika Christ, Anke Ernst, Juliane Folkerts, Jutta Hansmann, and Stefanie Klein. Krebs in deutschland 2011/2012. 2015.
- [LAS<sup>+</sup>05] Feng Li, Hidetaka Arimura, Kenji Suzuki, Junji Shiraishi, Qiang Li, Hiroyuki Abe, Roger Engelmann, Shusuke Sone, Heber MacMahon, and Kunio Doi. Computer-aided detection of peripheral lung cancers missed at ct: Roc analyses without and with localization 1. *Radiology*, 237(2):684–690, 2005.
- [LHF<sup>+</sup>01] Yongbum Lee, Takeshi Hara, Hiroshi Fujita, Shigeki Itoh, and Takeo Ishigaki. Automated detection of pulmonary nodules in helical ct images based on an improved template-matching technique. *IEEE Transactions on medical imaging*, 20(7):595–604, 2001.
- [LYC<sup>+</sup>16] Yixuan Li, Jason Yosinski, Jeff Clune, Hod Lipson, and John Hopcroft. Convergent learning: Do different neural networks learn the same representations? In *Proceedings of International Conference on Learning Representation (ICLR)*, 2016.
- [Mas11] D Mason. Su-e-t-33: Pydicom: An open source dicom library. *Medical Physics*, 38(6):3493–3493, 2011.
- [OCK05] Kazunori Okada, Dorin Comaniciu, and Arun Krishnan. Robust anisotropic gaussian fitting for volumetric characterization of pulmonary nodules in multislice ct. *IEEE Transactions on Medical Imaging*, 24(3):409–423, 2005.

- [OHO<sup>+</sup>13] Koji Ono, Toru Hiraoka, Asami Ono, Eiji Komatsu, Takehiko Shigenaga, Hajime Takaki, Toru Maeda, Hiroyuki Ogasu, Shintaro Yoshida, Kiyoyasu Fukushima, et al. Low-dose ct scan screening for lung cancer: comparison of images and radiation doses between low-dose ct and follow-up standard diagnostic ct. *SpringerPlus*, 2(1):393, 2013.
- [PGN<sup>+</sup>13] Paul F Pinsky, David S Gierada, P Hrudaya Nath, Ella Kazerooni, and Judith Amorosa. National lung screening trial: variability in nodule detection rates in chest ct studies. *Radiology*, 268(3):865–873, 2013.
- [Pia08] Oleg S. Pianykh. *A Brief History of DICOM*, pages 17–22. Springer Berlin Heidelberg, Berlin, Heidelberg, 2008.
- [PS17] Gregory Piatetsky-Shapiro. Getting started with deep learning, <https://www.kdnuggets.com/2017/03/getting-started-deep-learning.html>, 2017.
- [RSR04] Antoine Rosset, Luca Spadola, and Osman Ratib. Osirix: an open-source software for navigating in multidimensional dicom images. *Journal of digital imaging*, 17(3):205–216, 2004.
- [SAL<sup>+</sup>03] Kenji Suzuki, Samuel G Armato, Feng Li, Shusuke Sone, et al. Massive training artificial neural network (mtann) for reduction of false positives in computerized detection of lung nodules in low-dose computed tomography. *Medical physics*, 30(7):1602–1617, 2003.
- [SHK<sup>+</sup>14] Nitish Srivastava, Geoffrey E Hinton, Alex Krizhevsky, Ilya Sutskever, and Ruslan Salakhutdinov. Dropout: a simple way to prevent neural networks from overfitting. *Journal of machine learning research*, 15(1):1929–1958, 2014.
- [SSS<sup>+</sup>17] David Silver, Julian Schrittwieser, Karen Simonyan, Ioannis Antonoglou, Aja Huang, Arthur Guez, Thomas Hubert, Lucas Baker, Matthew Lai, Adrian Bolton, Yutian Chen, Timothy Lillicrap, Fan Hui, Laurent Sifre, George van den Driessche, Thore Graepel, and Demis Hassabis. Mastering the game of go without human knowledge. *Nature*, 550(7676):354–359, 10 2017.
- [SZY<sup>+</sup>15] Wei Shen, Mu Zhou, Feng Yang, Caiyun Yang, and Jie Tian. Multi-scale convolutional neural networks for lung nodule classification. In *International Conference on Information Processing in Medical Imaging*, pages 588–599. Springer, 2015.
- [TF13] Atsushi Teramoto and Hiroshi Fujita. Fast lung nodule detection in chest ct images using cylindrical nodule-enhancement filter. *International journal of computer assisted radiology and surgery*, pages 1–13, 2013.
- [TLD<sup>+</sup>09] Yimo Tao, Le Lu, Maneesh Dewan, Albert Y Chen, Jason Corso, Jianhua Xuan, Marcos Salganicoff, and Arun Krishnan. Multi-level ground glass nodule detection and segmentation in ct lung images. In *International Conference on Medical Image Computing and Computer-Assisted Intervention*, pages 715–723. Springer, 2009.

- [VC06] Carlos Vinhais and Aurélio Campilho. Lung parenchyma segmentation from ct images based on material decomposition. *Image Analysis and Recognition*, pages 624–635, 2006.
- [XAB02] Ning Xu, Narendra Ahuja, and Ravi Bansal. Automated lung nodule segmentation using dynamic programming and em based classification. In *Proc. SPIE*, volume 4684, pages 666–676, 2002.
- [XKM<sup>+</sup>97] Xin-Wei Xu, Takeshi Kobayashi, Heber MacMahon, Maryellen L Giger, et al. Development of an improved cad scheme for automated detection of lung nodules in digital chest images. *Medical Physics*, 24(9):1395–1403, 1997.
- [YLD<sup>+</sup>09] Xujiong Ye, Xinyu Lin, Jamshid Dehmeshki, Greg Slabaugh, and Gareth Beddoe. Shape-based computer-aided detection of lung nodules in thoracic ct images. *IEEE Transactions on Biomedical Engineering*, 56(7):1810–1820, 2009.
- [YTS<sup>+</sup>94] Shinji Yamamoto, Ippei Tanaka, Masahiro Senda, Yukio Tateno, Takeshi Iinuma, Toru Matsumoto, and Mitsuomi Matsumoto. Image processing for computer-aided diagnosis of lung cancer by ct (lsct). *Systems and Computers in Japan*, 25(2):67–80, 1994.

# **Declaration of Authorship**

I hereby certify that the work presented here is, to the best of my knowledge and belief, original and the result of my own investigations, except as acknowledged, and has not been submitted, either in part or whole, for a degree at this or any other university.

Osnabrück, December 8, 2017

